Supporting Information

Carrier-Fluid Screening for a 3-Phase Sublimation Refrigeration Cycle with CO_2 Using Reference Equations of State and COSMO-SAC

Erik Mickoleit, Andreas Jäger*, and Cornelia Breitkopf

Institute of Power Engineering, Faculty of Mechanical Science and Engineering, Technische Universität Dresden, Helmholtzstraße 14, 01069 Dresden, Germany

Corresponding Author

*E-mail: Andreas.Jaeger@tu-dresden.de

1 Choice of a Suitable Refrigeration Cycle

In this study, several CO_2 sublimation refrigeration cycles were investigated. The two basic setups investigated are:

1) A refrigeration cycle using a phase separator at intermediate pressure. CO_2 is used in the lower stage as well as in the upper stage.
2) A cascade refrigeration system with a different working fluid in the upper stage condensing at ambient temperature.

Different variants of these setups have been evaluated in order to find the most promising setup with the best efficiency. If the refrigeration system with alternative refrigerants has a lower efficiency compared to the state-of-the-art refrigeration cycles, the benefit of having a low GWP refrigerant might be outweighed by the additional greenhouse gas emissions due to higher electrical power demands. In industry, a common refrigeration cycle to achieve cooling temperatures below −50 °C is the R-23 cascade refrigeration cycle. Therefore, the R-23 cascade (see Figure S1) has been chosen as reference system. Prior to the screening of possible carrier-fluids, different options for refrigeration cycles are discussed in the following.

1.1 R23 Cascade as Basis Refrigeration Cycle

The cascade refrigeration cycle with R-23 in the lower stage, which is commonly used in industry, is chosen as the reference refrigeration cycle that all other options will be compared with. For the upper stage, R-404a (44% C_2HF_5, 52% $C_2H_3F_3$, 4% $C_2H_2F_4$, percentages given on a mass basis) has been chosen as this is a refrigerant that is currently used in such cascade refrigeration cycles. A flow chart of this cascade is illustrated in Figure S1.

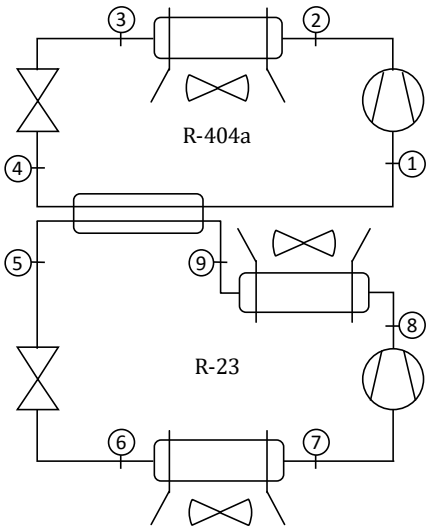

Figure S1: Flow chart of a common R-23/R-404a cascade refrigeration cycle

In the upper cycle, the superheated refrigerant R-404a is compressed from low pressure to high pressure by the compressor (state points 1-2). After the compressor outlet, the hot high-pressure gas is condensed and subcooled in the air-cooled condenser (2-3) before being expanded in an expansion valve to low pressure and low temperature (3-4). The refrigerant is then evaporated and superheated in the cascade heat exchanger (4-1). For this to happen, a heat source is needed in form of the lower stage via condensing and subcooling of R-23 on the other side of the cascade heat exchanger (9-5). From there, the R-23 expands to low pressure at temperatures of −75 °C (5-6). The "cooling power" is used in the evaporator through evaporating and superheating the R-23 (6-7) before it is compressed to high pressure by the compressor (7-8). After the compressor outlet, the high-pressure gas is cooled in an air-cooled heat exchanger (8-9) before reaching the cascade heat exchanger again.

1.2 CO_2 Sublimation Cascade

The cascade refrigeration cycle, as the most commonly used system to provide cooling below temperatures of −50 °C, has been used as basic setup for a CO_2 refrigeration system (see flow chart in Figure S2). Two modifications of this single-stage compression cascade are discussed in section 1.4.

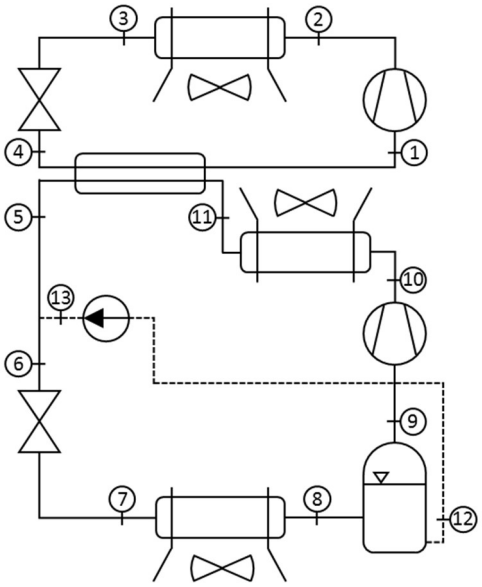

Figure S2: Flow chart of a CO_2 cascade refrigeration cycle with single-stage compression in lower stage and carrier-fluid phase separator

The operating principle is similar to the R-23 cascade mentioned in section 1.1. The upper stage resembles the upper stage of the state-of-the-art refrigeration cycle. However, instead of the refrigerant R-404a (GWP = 3922, according to the method of calculating the total GWP of a mixture[1]) R-134a (GWP = 1430[1]) has been used for the upper stage. The operating principle in the lower stage is also quite similar to the R-23 cascade. High-pressure gaseous CO_2 (or mixture with carrier-fluid) is condensed and subcooled in the cascade heat exchanger (see state points 11-5 of flow chart in Figure S2) using the "cooling power" of the upper stage (4-1). Subsequently, the liquid CO_2 (or mixture) is mixed with the carrier-fluid (containing dissolved CO_2) (6) before expanding to low pressure (7). A 3-phase expansion occurs in the expansion valve, where the liquid phase is intended to help avoiding blockages in and after the expansion valve. Furthermore, the heat transfer in the sublimator may be improved by the presence of a liquid phase. In this configuration, a sublimator instead of an evaporator is used as heat exchanger at low pressure (7-8). A low-pressure carrier-fluid separator is used after the sublimator (8). This component is needed to separate the gaseous CO_2 (9) after sublimation from the liquid carrier-fluid (12). However, note that the gaseous phase contains a certain amount of the carrier-fluid and small amounts of CO_2 dissolve in the liquid phase. With the use of a pump (12-13), the separated carrier-fluid is mixed again with the liquid CO_2 before expansion.

1.3 CO_2 Sublimation Cycle with Intermediate Pressure Phase Separator

Instead of utilizing a cascade with two separate cycles connected via a heat exchanger, CO_2 could be used as refrigerant in the entire system. For this configuration, an intermediate pressure phase separator will come into place to reduce the mass flow of gaseous CO_2 (or mixture with carrier-fluid) in the lower stage of the cycle. In this setup (see Figure S3), the condensed and subcooled CO_2 (or mixture) (3) is expanded into a phase separator to an intermediate pressure p_4 (3-4). In the basic setup (Figure S3), the liquid phase (6) is expanded to low pressure p_8 (8). The sublimation occurs in the sublimator heat exchanger (8-9). After superheating in the sublimator, the gaseous CO_2 (or mixture) is compressed to the intermediate pressure p_4 (11)

with a single-stage compressor and then recooled in an air-cooled heat exchanger (11-12) before it is mixed with the saturated vapor of CO_2 (or mixture) from the phase separator (1). The gaseous CO_2 (or mixture) then flows to the compressor inlet to be compressed to the condensation pressure p_2 (2) and the cycle starts again.

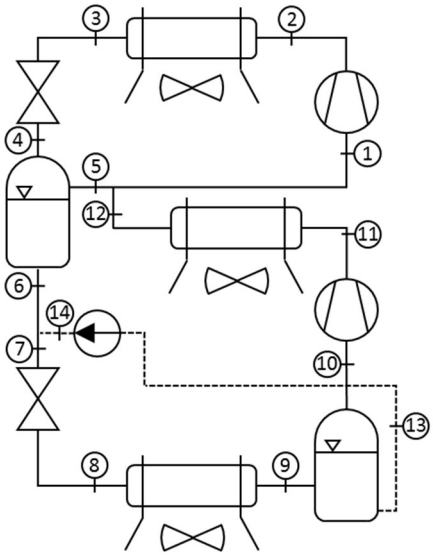

Figure S3: Flow chart of a CO_2 sublimation cycle with intermediate pressure phase separator, single-stage compression in lower stage and carrier-fluid phase separator

1.4 Modifications of the Basic Setups

Two-stage compression in lower stage

The first modification is the use of a two-stage compression in the lower stages of the systems of both basic setups (according to Figure S2 and Figure S3). The reasons are the large pressure ratios of sublimation pressure to condensation pressure (intermediate pressure phase separator setup) or intermediate pressure (cascade setup). The modifications are shown on the left hand sides of Figure S4 and Figure S5. A lower pressure ratio in each compressor will result in better isentropic efficiencies (which are assumed to be a function of the pressure ratio in this work) and therefore a better COP is to be expected. The lower inlet temperature at the second compressor (11-12 in Figure S4 (left), 12-13 in Figure S5 (left)) due to the use of a recooler also reduces the required power for compression. Besides these modifications, the remaining setups are identical to the basic setups.

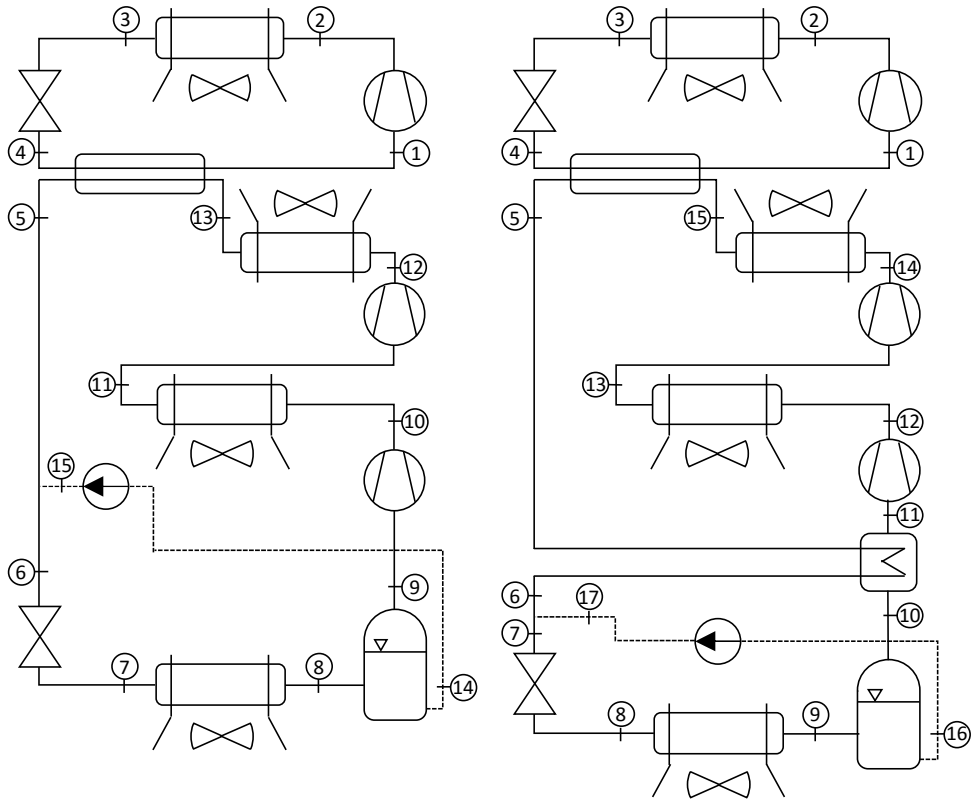

Figure S4: CO_2 cascade refrigeration cycles with two-stage compression (left) and two-stage compression in lower stage with internal heat exchanger (IHE) (right).

Two-stage compression in lower stage and internal heat exchanger

Additionally, a widely used method of improving the COP in refrigeration cycles is using an internal heat exchanger (IHE) to reduce the temperature of the high-pressure liquid refrigerant (5-6 in Figure S4 (right), 6-7 in Figure S5 (right)). For this, the low-pressure sublimated cold CO_2 (or mixture) is superheated in the internal heat exchanger while subcooling the liquid CO_2 (or mixture). The IHE is not only important for enhancing the COP. It is also important from a technical standpoint to increase the compressor inlet temperature of the sublimated CO_2, as at temperatures of about 198 K cold embrittlement of parts of the compressor could occur. This might reduce lifetime of the compressor and can be avoided by using an IHE in order to heat the CO_2 (or mixture) before entering the compressor. For all further investigations, the compressor inlet temperature has been (arbitrarily) set to 252.15 K.

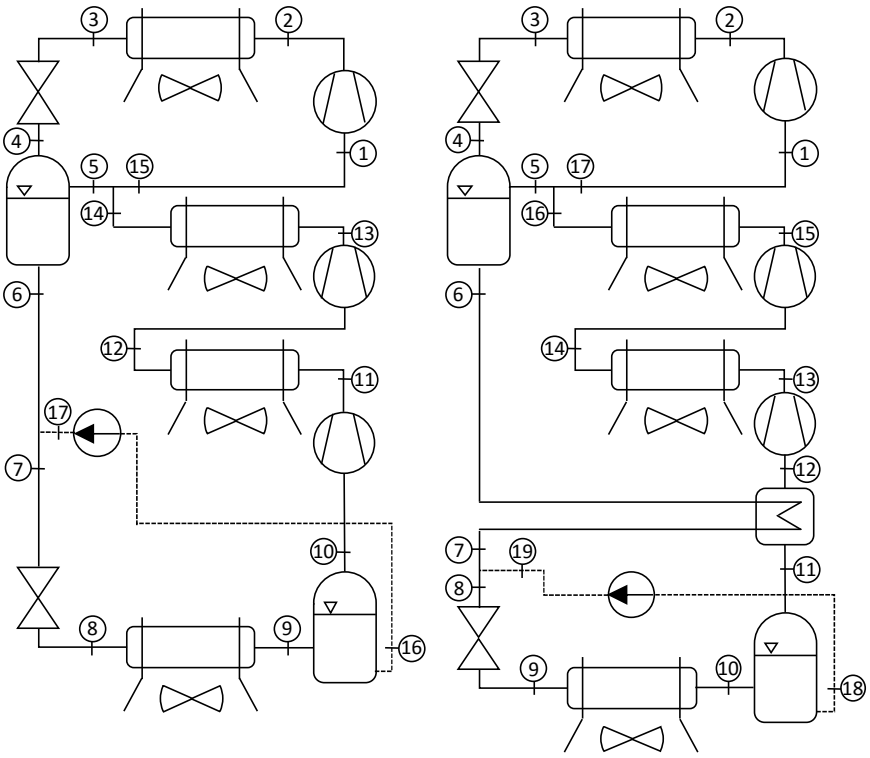

Figure S5: CO_2 sublimation cycles with two-stage compression (left) and two-stage compression in lower stage with IHE (right)

1.5 Selection of a suitable option

Both setups, the cascade and the phase separator at intermediate pressure, have certain advantages and disadvantages, which are discussed in the following. One of the mayor challenges when using CO_2 as refrigerant are high working pressures. This is especially the case, when condensation with an air-cooled heat exchanger is intended. At 20 °C, the condensation pressure of pure CO_2 is 5.729 MPa[2]. Design and tightness of high-pressure components are manageable but require higher investment costs compared to state-of-the-art refrigeration cycles. With the critical temperature of CO_2 at about 31 °C being very close to ambient temperature conditions for many regions in the world, operating at summer conditions might become problematic, as CO_2 will be supercritical above this temperature. These considerations would have to be taken into account, when choosing the option with CO_2 in the entire system (Figure S3 and Figure S5). However, an advantage of this option is that no heat exchanger is needed for connecting the lower and the upper stage of this refrigeration cycle. The main advantage of having a separate upper stage in the cascade setup is that another refrigerant can be used with a vapor-pressure curve more suited for ambient temperature conditions compared to CO_2.

To get an overview of expected theoretical COPs of such refrigeration cycles, thermodynamic calculations using the thermodynamic reference database TREND 3.0[3] were undertaken for pure CO_2, using the reference equation of state for CO_2[2] and the equation of state for solid CO_2 by Jäger and Span[4] in order to calculate the required thermophysical properties. The results are illustrated in Figure S6. The boundary conditions for all calculations are given in Table S1.

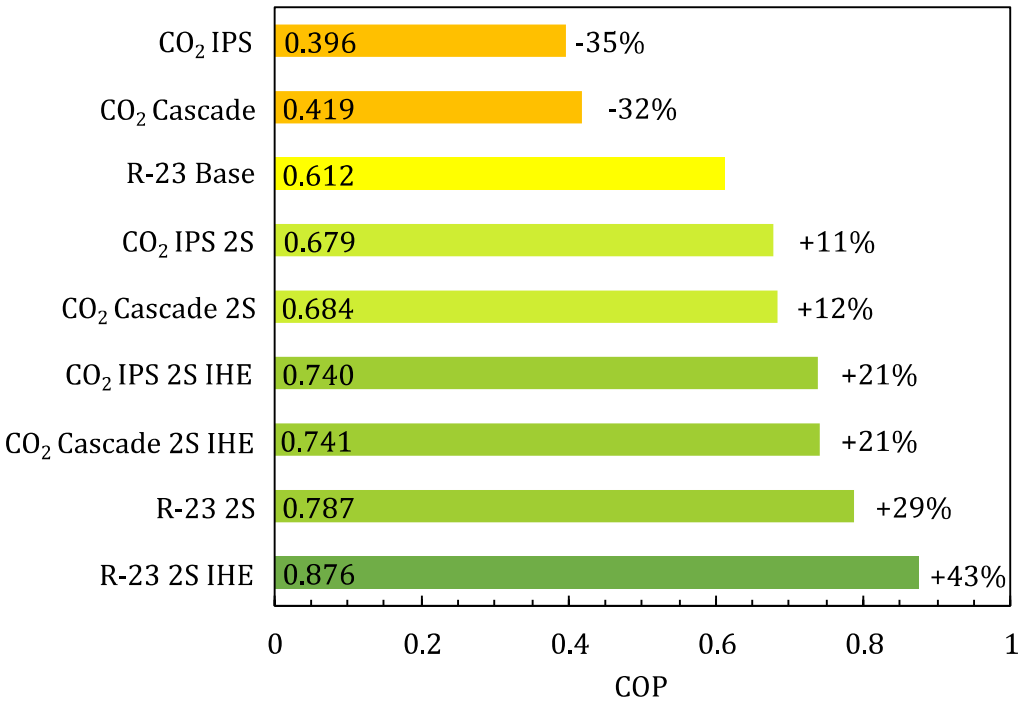

Figure S6: COPs of different configurations of the CO_2 sublimation cycle with intermediate pressure phase separator (CO_2 IPS) and CO_2 cascade single stage (CO_2 Cascade), two stage (2S) with and without internal heat exchanger (IHE) compared to R23 cascade as single stage (R-23 Base), two stage compression with IHE (R-23 2S IHE) and without IHE (R-23 2S).

Table S1: Boundary conditions for thermodynamic refrigeration cycle calculations

Temperatures	
Ambient temperature T_{amb}	295.15 K
Sublimation temperature	198.15 K
Compressor inlet temperature	252.15 K
Condensation temperature at cascade heat exchanger T_{cas}	261.00 K
Heat exchanger temperature gradients	
Condenser upper stage ΔT_{con}	10 K
Intercooler ΔT_{IC}	10 K
Cascade ΔT_{cas}	7 K
Internal heat exchanger	7 K
Subcooling or overheating	
Subcooling ΔT_{sc}	3 K
Overheating ΔT_{oh}	5 K
pressure ratio Π	
Single stage	13.363
Two stage	4.709
isentropic efficiencies η	
All compressors	$\eta_s = 0.875 - 0.0375 \cdot \Pi$

Figure S6 shows that the difference in the expected COPs between the setups with intermediate pressure phase separator and the cascade are rather small. Hence, due to the discussed disadvantages of the setup with intermediate pressure phase separator, the cascade refrigeration system with two stage compression and internal heat exchanger (Figure S4, right) has been chosen for the screening.

2 Comparison to Experimental Data

The validation of the predictive multi-fluid mixture model in combination with COSMO-SAC as g^E-model has been done in a previous work for ten different binary mixtures[5]. This section deals with the comparison of the proposed model to experimental phase equilibrium data for each binary mixture of CO_2 with methane, ethane, propane, methanol, and ethanol on different isotherms. For all components, multiparameter equations of state[2,6–10] have been used. The results can be seen in Figures Figure **S7** to Figure **S11**. The solid black lines represent calculated phase equilibria using the predictive multi-fluid mixture model with COSMO-SAC as g^{E}-model. This mixture model relies on a theoretical formulation of the departure function of the multi-fluid mixture model[11]. The grey dashed lines represent the results calculated from the multi-fluid mixture model with linear mixing rules, as also discussed in our previous work[5,11]. All calculations have been done using the thermophysical property software TREND[12]. All model results are compared with experimental data from the literature: CO_2 + methane[13], CO_2 + ethane[14–17], CO_2 + propane[18,19], CO_2 + methanol[20–28], and CO_2 + ethanol[23–25,27–36].

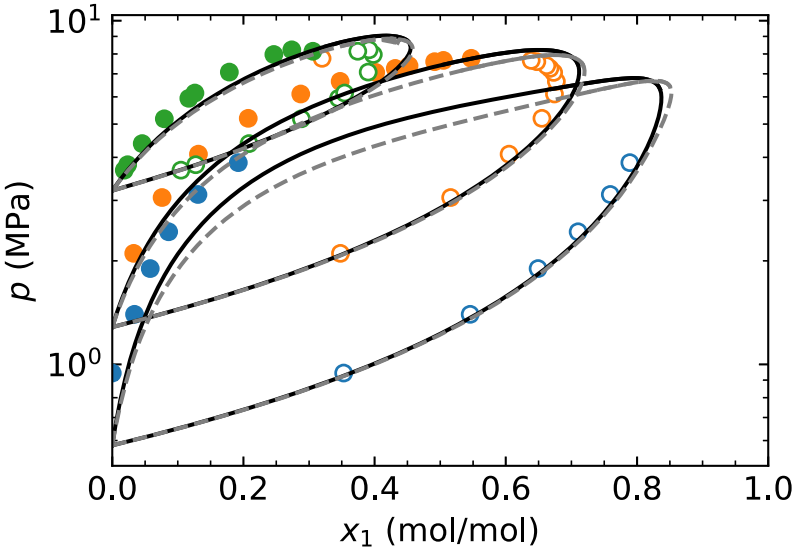

Figure S7: Experimental VLE data (symbols) for the binary mixture of CO_2 + methane and phase equilibria calculated with the multi-fluid mixture model combined with COSMO-SAC (black solid lines) for the isotherms at 219.27 K, 240.01 K, and 270 K. The grey dashed lines represent phase equilibria calculated with the multi-fluid mixture model with linear mixing rules.

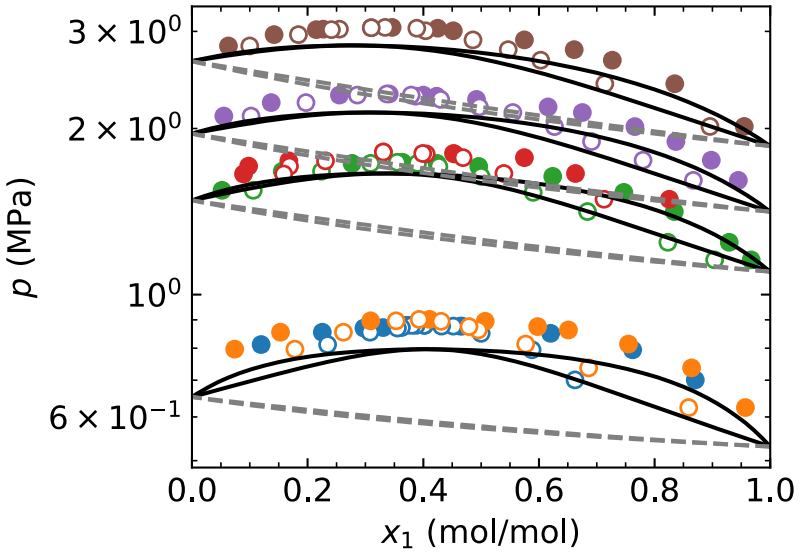

Figure S8: Experimental VLE data (symbols) for the binary mixture of CO_2 + ethane and phase equilibria calculated with the multi-fluid mixture model combined with COSMO-SAC (black solid lines) for the isotherms at 222.05 K, 244.27 K, 252.95 K, and 263.15 K. The grey dashed lines represent phase equilibria calculated with the multi-fluid mixture model with linear mixing rules.

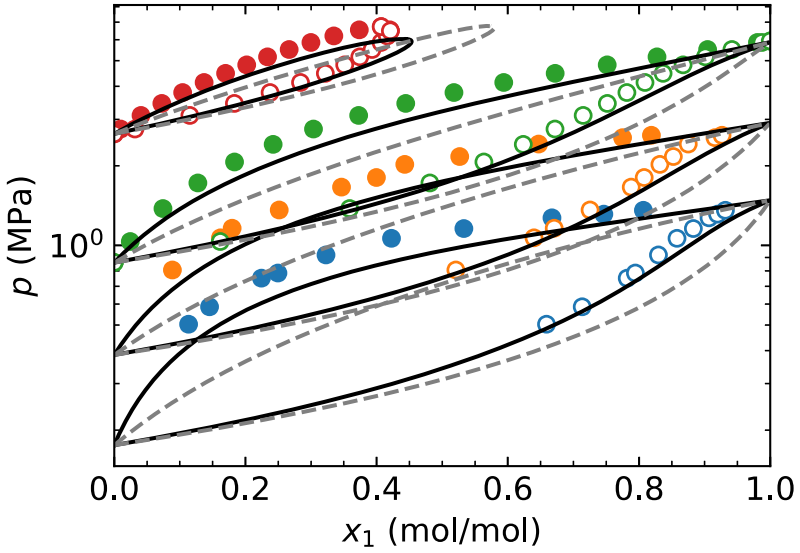

Figure S9: Experimental VLE data (symbols) for the binary mixture of CO_2 + propane and phase equilibria calculated with the multi-fluid mixture model combined with COSMO-SAC (black solid lines) for the isotherms at 244.26 K, 266.48 K, 294.26 K, and 344.26 K. The grey dashed lines represent phase equilibria calculated with the multi-fluid mixture model with linear mixing rules.

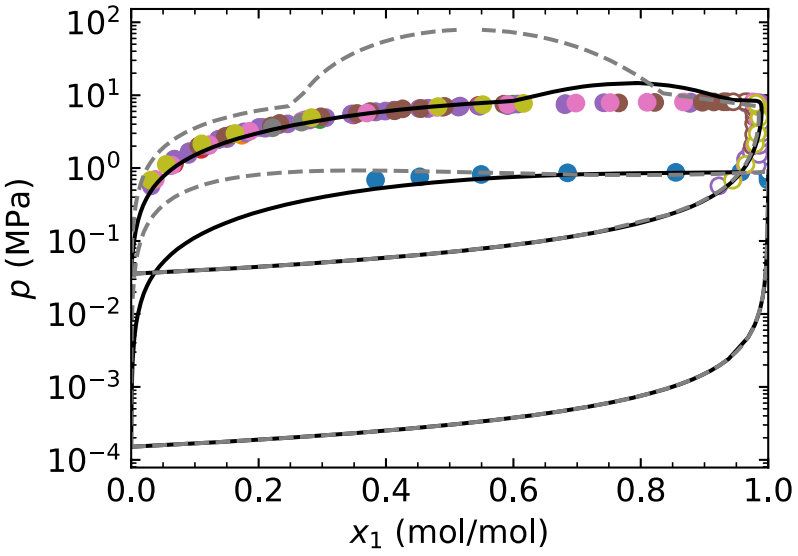

Figure S10: Experimental VLE data (symbols) for the binary mixture of CO_2 + methanol and phase equilibria calculated with the multi-fluid mixture model combined with COSMO-SAC (black solid lines) for the isotherms at 230 K and 313.14 K. The grey dashed lines represent phase equilibria calculated with the multi-fluid mixture model with linear mixing rules. Note that the minimum and maximum of the bubble line at 230 K (of the multi-fluid mixture model with linear mixing rules, i.e., grey dashed lines) indicates metastable VLE.

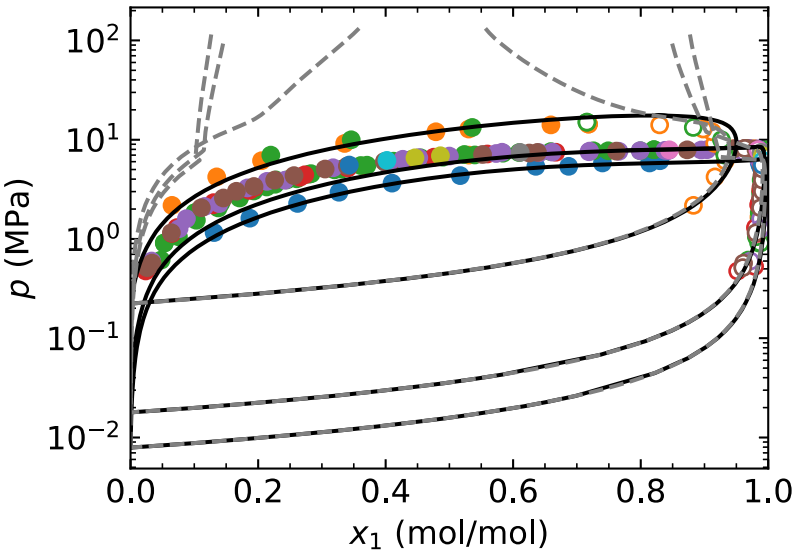

Figure S11: Experimental VLE data (symbols) for the binary mixture of CO_2 + ethanol and phase equilibria calculated with the multi-fluid mixture model combined with COSMO-SAC (black solid lines) for the isotherms at 298.17 K, 313.14 K, and 373 K. The grey dashed lines represent phase equilibria calculated with the multi-fluid mixture model with linear mixing rules. At pressures higher than 100 MPa, the calculations have been aborted.

References

(1) Regulation (EU) No 517/2014 of the European Parliament and of the Council of 16 April 2014 on Fluorinated Greenhouse Gases L 150. **2014**.

(2) Span, R.; Wagner, W. A New Equation of State for Carbon Dioxide Covering the Fluid Region from the Triple-Point Temperature to 1100 K at Pressures up to 800 MPa. *J. Phys. Chem. Ref. Data* **1996**, *25*, 1509–1596. https://doi.org/10.1063/1.555991.

(3) Span, R.; Eckermann, T.; Herrig, S.; Hielscher, S.; Jäger, A.; Thol, M. *TREND. Thermodynamic Reference and Engineering Data 3.0*; Lehrstuhl fuer Thermodynamik, Ruhr-Universitaet Bochum: Bochum, Germany, 2016.

(4) Jäger, A.; Span, R. Equation of State for Solid Carbon Dioxide Based on the Gibbs Free Energy. *J. Chem. Eng. Data* **2012**, *57*, 590–597. https://doi.org/10.1021/je2011677.

(5) Jäger, A.; Mickoleit, E.; Breitkopf, C. A Combination of Multi-Fluid Mixture Models with COSMO-SAC. *Fluid Phase Equilib.* **2018**, *476*, 147–156. https://doi.org/10.1016/j.fluid.2018.08.004.

(6) Schroeder, J. A.; Penoncello, S. G.; Schroeder, J. S. A Fundamental Equation of State for Ethanol. *J. Phys. Chem. Ref. Data* **2014**, *43*, 043102. https://doi.org/10.1063/1.4895394.

(7) Setzmann, U.; Wagner, W. A New Equation of State and Tables of Thermodynamic Properties for Methane Covering the Range from Melting Line to 625 K at Pressures up to 1000 MPa. *J. Phys. Chem. Ref. Data* **1991**, *20*, 1061–1155.

(8) Bücker, D.; Wagner, W. A Reference Equation of State for the Thermodynamic Properties of Ethane for Temperatures from the Melting Line to 675 K and Pressures up to 900 MPa. *J. Phys. Chem. Ref. Data* **2006**, *35*, 205–266. https://doi.org/10.1063/1.1859286.

(9) Lemmon, E. W.; McLinden, M. O.; Wagner, W. Thermodynamic Properties of Propane. III. A Reference Equation of State for Temperatures from the Melting Line to 650 K and Pressures up to 1000 MPa. *J. Chem. Eng. Data* **2009**, *54*, 3141–3180. https://doi.org/10.1021/je900217v.

(10) de Reuck, K. M.; Craven, R. J. B. *Methanol, International Thermodynamic Tables of the Fluid State - 12*; IUPAC, Blackwell Scientific Publications: London, 1993.

(11) Jäger, A.; Bell, I. H.; Breitkopf, C. A Theoretically Based Departure Function for Multi-Fluid Mixture Models. *Fluid Phase Equilib.* **2018**, *469*, 56–69. https://doi.org/10.1016/j.fluid.2018.04.015.

(12) Span, R.; Eckermann, T.; Herrig, S.; Hielscher, S.; Jäger, A.; Mickoleit, E.; Neumann, T.; Pohl, S.; Semrau, B.; Thol, M. *TREND. Thermodynamic Reference and Engineering Data 4.0.*; Lehrstuhl fuer Thermodynamik, Ruhr-Universitaet Bochum: Bochum, Germany, 2019.

(13) Al-Sahhaf, T. A.; Kidnay, A. J.; Sloan, E. D. Liquid + Vapor Equilibria in the Nitrogen + Carbon Dioxide + Methane System. *Ind. Eng. Chem. Fundam.* **1983**, *22*, 372–380. https://doi.org/10.1021/i100012a004.

(14) Nagahama, K.; Konishi, H.; Hoshino, D.; Hirata, M. Binary Vapor-Liquid Equilibria Of Carbon Dioxide-Llight Hydrocarbons At Low Temperature. *Journal of Chemical Engineering of Japan* **1974**, *7*, 323–328. https://doi.org/10.1252/jcej.7.323.

(15) Hamam, S. E. M.; Lu, B. C. Y. Vapor-liquid Equilibrium in the Ethane-carbon Dioxide System. *Can. J. Chem. Eng.* **1974**, *52*, 283–286. https://doi.org/10.1002/cjce.5450520226.

(16) Fredenslund, A.; Mollerup, J. Measurement and Prediction of Equilibrium Ratios for the C_2H_6+CO_2 System. *J. Chem. Soc., Faraday Trans. 1* **1974**, *70*, 1653–1660.

(17) Fredenslund, A.; Mollerup, J.; Hall, K. R. Vapor-Liquid-Equilibrium Data for Systems C_2H_4+C_2H_6 and CO_2+C_2H_4+C_2H_6. *J. Chem. Eng. Data* **1976**, *21*, 301–304. https://doi.org/10.1021/je60070a006.

(18) Hamam, S. E. M.; Lu, B. C. Y. Isothermal Vapor-Liquid Equilibriums in Binary System Propane-Carbon Dioxide. *J. Chem. Eng. Data* **1976**, *21*, 200–204. https://doi.org/10.1021/je60069a020.

(19) Reamer, H.; Sage, B.; Lacey, W. Phase Equilibria in Hydrocarbon Systems - Volumetric and Phase Behavior. *Ind. Eng. Chem.* **1951**, *43*, 2515–2520. https://doi.org/10.1021/ie50503a035.

(20) Hong, J. H.; Kobayashi, R. Vapor—Liquid Equilibrium Studies for the Carbon Dioxide—Methanol System. *Fluid Phase Equilibria* **1988**, *41*, 269–276. https://doi.org/10.1016/0378-3812(88)80011-6.
(21) Elbaccouch, M. M.; Raymond, M. B.; Elliott, J. R. High-Pressure Vapor−Liquid Equilibrium for R-22 + Ethanol and R-22 + Ethanol + Water. *J. Chem. Eng. Data* **2000**, *45*, 280–287. https://doi.org/10.1021/je990136g.
(22) Chang, C. J.; Day, C.-Y.; Ko, C.-M.; Chiu, K.-L. Densities and P-x-y Diagrams for Carbon Dioxide Dissolution in Methanol, Ethanol, and Acetone Mixtures. *Fluid Phase Equilibria* **1997**, *131*, 243–258. https://doi.org/10.1016/S0378-3812(96)03208-6.
(23) Chang, C. J.; Chiu, K.-L.; Day, C.-Y. A New Apparatus for the Determination of P–x–y Diagrams and Henry's Constants in High Pressure Alcohols with Critical Carbon Dioxide. *J. Supercrit. Fluids* **1998**, *12*, 223–237. https://doi.org/10.1016/S0896-8446(98)00076-X.
(24) Tochigi, K.; Namae, T.; Suga, T.; Matsuda, H.; Kurihara, K.; dos Ramos, M. C.; McCabe, C. Measurement and Prediction of High-Pressure Vapor–Liquid Equilibria for Binary Mixtures of Carbon Dioxide+n-Octane, Methanol, Ethanol, and Perfluorohexane. *J. Supercrit. Fluids* **2010**, *55*, 682–689. https://doi.org/10.1016/j.supflu.2010.10.016.
(25) Joung, S. N.; Yoo, C. W.; Shin, H. Y.; Kim, S. Y.; Yoo, K.-P.; Lee, C. S.; Huh, W. S. Measurements and Correlation of High-Pressure VLE of Binary CO2–Alcohol Systems (Methanol, Ethanol, 2-Methoxyethanol and 2-Ethoxyethanol). *Fluid Phase Equilib.* **2001**, *185*, 219–230. https://doi.org/10.1016/S0378-3812(01)00472-1.
(26) Kodama, D.; Kubota, N.; Yamaki, Y.; Tanaka, H.; Kato, M. High Pressure Vapor-Liquid Equilibria and Density Behaviors for Carbon Dioxide + Methanol System at 313.15. *Netsu Bussei* **1996**, *10*, 16–20. https://doi.org/10.2963/jjtp.10.16.
(27) Yoon, J. H.; Lee, H. S.; Lee, H. High-Pressure Vapor-Liquid Equilibria for Carbon Dioxide + Methanol, Carbon Dioxide + Ethanol, and Carbon Dioxide + Methanol + Ethanol. *Journal of Chemical & Engineering Data* **1993**, *38*, 53–55. https://doi.org/10.1021/je00009a012.
(28) Suzuki, K.; Sue, H.; Itou, M.; Smith, R. L.; Inomata, H.; Arai, K.; Saito, S. Isothermal Vapor-Liquid Equilibrium Data for Binary Systems at High Pressures: Carbon Dioxide-Methanol, Carbon Dioxide-Ethanol, Carbon Dioxide-1-Propanol, Methane-Ethanol, Methane-1-Propanol, Ethane-Ethanol, and Ethane-1-Propanol Systems. *J. Chem. Eng. Data* **1990**, *35*, 63–66. https://doi.org/10.1021/je00059a020.
(29) Day, C.-Y.; Chang, C. J.; Chen, C.-Y. Phase Equilibrium of Ethanol + CO2 and Acetone + CO2 at Elevated Pressures. *J. Chem. Eng. Data* **1996**, *41*, 839–843. https://doi.org/10.1021/je960049d.
(30) Galicia-Luna, L. A.; Ortega-Rodriguez, A.; Richon, D. New Apparatus for the Fast Determination of High-Pressure Vapor−Liquid Equilibria of Mixtures and of Accurate Critical Pressures. *J. Chem. Eng. Data* **2000**, *45*, 265–271. https://doi.org/10.1021/je990187d.
(31) Secuianu, C.; Feroiu, V.; Geană, D. Phase Behavior for Carbon Dioxide+ethanol System: Experimental Measurements and Modeling with a Cubic Equation of State. *J. Supercrit. Fluids* **2008**, *47*, 109–116. https://doi.org/10.1016/j.supflu.2008.08.004.
(32) Knez, Ž.; Škerget, M.; Ilič, L.; Lütge, C. Vapor–Liquid Equilibrium of Binary CO2–Organic Solvent Systems (Ethanol, Tetrahydrofuran, Ortho-Xylene, Meta-Xylene, Para-Xylene). *J. Supercrit. Fluids* **2008**, *43*, 383–389. https://doi.org/10.1016/j.supflu.2007.07.020.
(33) Lim, J. S.; Lee, Y. Y.; Chun, H. S. Phase Equilibria for Carbon Dioxide-Ethanol-Water System at Elevated Pressures. *J. Supercrit. Fluids* **1994**, *7*, 219–230. https://doi.org/10.1016/0896-8446(94)90009-4.
(34) Tsivintzelis, I.; Missopolinou, D.; Kalogiannis, K.; Panayiotou, C. Phase Compositions and Saturated Densities for the Binary Systems of Carbon Dioxide with Ethanol and Dichloromethane. *Fluid Phase Equilibria* **2004**, *224*, 89–96. https://doi.org/10.1016/j.fluid.2004.06.046.
(35) Jennings, D. W.; Lee, R. J.; Teja, A. S. Vapor-Liquid Equilibria in the Carbon Dioxide + Ethanol and Carbon Dioxide + 1-Butanol Systems. *J. Chem. Eng. Data* **1991**, *36*, 303–307. https://doi.org/10.1021/je00003a013.

(36) Pfohl, O.; Pagel, A.; Brunner, G. Phase Equilibria in Systems Containing O-Cresol, p-Cresol, Carbon Dioxide, and Ethanol at 323.15–473.15 K and 10–35 MPa. *Fluid Phase Equilib.* **1999**, *157*, 53–79. https://doi.org/10.1016/S0378-3812(99)00019-9.